XLVI CILAMCE
VITÓRIA - ES - BRAZIL - 2025
XLVI IBERO-LATIN AMERICAN CONGRESS ON COMPUTATIONAL METHODS IN ENGENEERING

Inverse Analysis for Estimating Temperature-Dependent Thermal Properties in Orthotropic Media using Differential Evolution

David L. S. Rodrigues[1], Felipe S. Loureiro[1], Rafael R. S. Melo[1], Gustavo R. Souza[1], Michelli M. S. Loureiro[2]

[1]*Dept. of Thermal and Fluid Sciences, Federal University of São João del-Rei*
Praça Frei Orlando, 170, 36307-352, São João del-Rei/MG, Brazil
rsdavid35@aluno.ufsj.edu.br, felipe.loureiro@ufsj.edu.br, rafaelmelo@ufsj.edu.br, souzagr@ufsj.edu.br
[2]*Dept. of Computer Science, Federal University of São João del-Rei*
Av. Visc. do Rio Preto, S/N, 36301-360, São João del-Rei/MG, Brazil
michelli.loureiro@ufsj.edu.br

Abstract. Inverse heat conduction analysis plays an important role in estimating material properties, especially in complex thermal systems where direct measurement is challenging. In this study, the differential evolution algorithm is employed to minimize the objective function, which is defined as the ordinary least squares error of the real values and the predicted ones, of the inverse problem in a two-dimensional orthotropic medium. Thus, the inverse problem consists in estimating the two components of the thermal conductivity tensor and the heat capacity, both of which are assumed to be temperature-dependent functions. The direct problem governed by the transient nonlinear heat conduction model is numerically solved by a developed code based on the FEM through the implicit Euler scheme and the Picard iteration method. The solution of the inverse problem, both with and without noise in the simulated data, demonstrates that accurate outcomes are achieved, indicating a robust and simple methodology for estimating the thermophysical parameters.

Keywords: Inverse heat conduction, Differential evolution, Orthotropic materials, Nonlinear FEA, Transient analysis

1 Introduction

The determination of thermophysical properties in orthotropic materials, where the properties vary with directions, can be resolved by solving an inverse problem [1–3]. This approach consists of estimating the unknown properties based on given experimental temperature data. For this, mathematical and computational modeling of the problem under consideration is performed, and parameters that minimize the error between the model's temperature field and the experimental temperature data are obtained by optimizing an objective function. Both deterministic and stochastic techniques can be employed for such a purpose [4].

As opposed to traditional deterministic methods frequently used in solving inverse heat conduction problems, evolutionary algorithms have gained great popularity due to their numerous advantages such as global search capability, no need of gradient calculation, and parallelism and scalability. Among these, the Differential Evolution (DE) algorithm is comparatively less utilized in inverse heat transfer problems than other ones such as Genetic Algorithms or the Particle Swarm Optimization (PSO) algorithm [4–7]. Therefore, the objective of this work is to employ the DE algorithm to estimate the heat capacity and the components of the thermal conductivity tensor of an orthotropic material, both assumed to vary linearly with temperature, similar to the case studied by Sawaf et al. [8]. However, the direct problem is solved by the finite element method using an in-house MATLAB code, while the inverse problem is tackled through three distinct common variants of the Differential Evolution algorithm. To evaluate the robustness of the proposed methodology, both noise-free computational experiments and noisy simulated data, reflecting measurement errors from the real experiment conducted by Kim et al. [3], are employed.

2 Inverse problem statement

The bi-dimensional transient heat transfer in an orthotropic solid represented by the domain $\Omega\,(x, y) = (0, a) \times (0, b)$ is considered as depicted in Fig. 1. The transient nonlinear heat transfer equation is given as

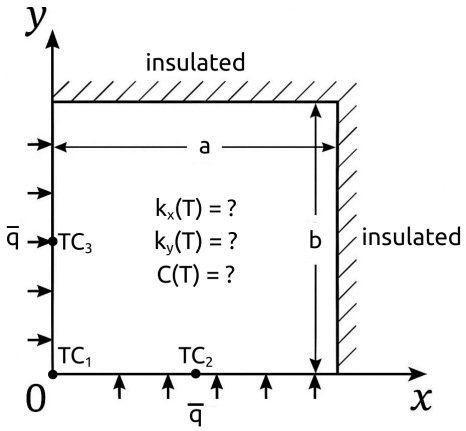


Figure 1. Schematic representation of the inverse problem

follows:

$$C(T)\frac{\partial T}{\partial t} = \frac{\partial}{\partial x}\left(k_x(T)\frac{\partial T}{\partial x}\right) + \frac{\partial}{\partial y}\left(k_y(T)\frac{\partial T}{\partial y}\right) \text{ in } \Omega \text{ for } t > 0 \tag{1}$$

where $k_x(T)$ and $k_y(T)$ are thermal conductivities in the x and y directions, respectively, and $C(T)$ is the volumetric heat capacity. These properties vary with the temperature according eq. (2):

$$k_x(T) = k_{x0} + k_{x1}T;\ k_y(T) = k_{y0} + k_{y1}T;\ C(T) = C_0 + C_1T. \tag{2}$$

The boundary and initial conditions are:

$$-k_x(T)\frac{\partial T}{\partial x} = \bar{q} \text{ at } x = 0;\ -k_y(T)\frac{\partial T}{\partial y} = \bar{q} \text{ at } y = 0,\ \text{for } t > 0 \tag{3}$$

$$\frac{\partial T}{\partial x} = 0 \text{ at } x = a;\ \frac{\partial T}{\partial y} = 0 \text{ at } y = b, \text{for } t > 0 \tag{4}$$

$$T = T_0 \text{ in } \Omega \text{ for } t = 0 \tag{5}$$

where $\bar{q}$ is the prescribed heat flux, and T_0 is the initial condition of the model.

In the present model, the parameter values k_{x0}, k_{x1}, k_{y0}, k_{y1}, C_0 and C_1 are unknown. Therefore, the inverse problem consists of estimating the parameter vector $\mathbf{X} = [k_{x0}, k_{x1}, k_{y0}, k_{y1}, C_0, C_1]$ taking into account the following additional information concerning experimental data measured at different thermocouples.

$$Y\left(TC_i, t_j\right),\ i = 1, \ldots, N_s;\ j = 1, \ldots, N_t \tag{6}$$

where $Y(TC_i, t_j)$ is the experimentally measured temperature at the thermocouple position TC_i in the time instant t_j. Finally, N_s is the number of thermocouples and N_t is the number of experimental measures. Here, three thermocouples (i.e., $N_s = 3$) placed at points $TC_1 = (0.0, 0.0)$, $TC_2 = (0.5a, 0.0)$ and $TC_3 = (0.0, 0.5b)$ are considered (see Fig. 1). The entire configuration was based on the work of Sawaf et al. [8].

3 Solution of the inverse problem

The objective function concerning the inverse problem is defined as:

$$S(\mathbf{X}) = \sum_{i=1}^{N_s}\sum_{j=1}^{N_t}(Y(TC_i, t_j) - T(TC_i, t_j; \mathbf{X}))^2 \tag{7}$$

where $T(TC_i, t_j; \mathbf{X})$ is the temperature calculated from the direct problem at the thermocouple position TC_i in time t_j taking into account an estimated parameter vector $\mathbf{X} \in \mathbb{R}^D$ with $D = 6$ being the dimension of the problem. Here, the Differential Evolution algorithm [9] is employed to minimize eq. (7); therefore, the inverse problem is formulated as the following minimization problem:

$$\begin{aligned} &\min_{\mathbf{X}\in\mathbb{R}^D} S(\mathbf{X}), \quad X_j^L \le X_j \le X_j^U,\ j=1,\ldots,D \\ &s.t.\ k_x(T)>0;\ k_y(T)>0;\ C(T)>0 \end{aligned} \tag{8}$$

where $\mathbf{X}^L \in \mathbb{R}^6$ and $\mathbf{X}^U \in \mathbb{R}^6$ are the lower and upper bound vectors, respectively.

After the initial population of size N_{pop} is randomly generated in the search space, i.e., $\mathbf{X}_i^{it},\ i=1,\ldots,N_{pop}$, the Differential Evolution algorithm primarily consists of three steps: mutation, crossover, and selection. In the mutation, for each vector $\mathbf{X}_i^{it}$, a vector $\mathbf{V}_i^{it}$ composed of the combination of $\mathbf{X}_b^{it}$, $\mathbf{X}_{r_1}^{it}$, $\mathbf{X}_{r_2}^{it}$, $\mathbf{X}_{r_3}^{it}$, $\mathbf{X}_{r_4}^{it}$ and $\mathbf{X}_{r_5}^{it}$ is formed, where r_1, r_2, r_3, r_4, r_5 are random integer numbers in the interval $[1, N_{pop}]$ different from each other as well as different from i, and $\mathbf{X}_b^{it}$ is the current best individual. This operator is carried out in a unified manner through eq. (9) as proposed in the work of Qiang and Mitchell [10].

$$\mathbf{V}_i^{it} = \mathbf{X}_i^{it} + F_1(\mathbf{X}_b^{it} - \mathbf{X}_i^{it}) + F_2(\mathbf{X}_{r_1}^{it} - \mathbf{X}_i^{it}) + F_3(\mathbf{X}_{r_2}^{it} - \mathbf{X}_{r_3}^{it}) + F_4(\mathbf{X}_{r_4}^{it} - \mathbf{X}_{r_5}^{it}) \tag{9}$$

where F_1, F_2, F_3, F_4 are real numbers that belong to the interval $[0,1]$, and their values determine the variant of the DE algorithm according to Tab. 1.

Table 1. DE variants according to the F_k parameters.

	F_1	F_2	F_3	F_4
DE/rand/1/bin	0.0	1.0	F	0.0
DE/best/1/bin	1.0	0.0	F	0.0
DE/current-to-best/1/bin	F	0.0	F	0.0

The variant *DE/rand/1/bin* is more exploratory, while *DE/best/1/bin* has the advantage of exploitation. The *DE/current-to-best/1/bin* variant aims to balance these two characteristics. Also, the F parameters are real scale factors and their determination is not a consensus in the literature. However, according to Qiang and Mitchell [10], $F = 0.9$ for *DE/rand/1/bin* and $F = 0.6$ for *DE/best/1/bin* are reasonable choices. In addition, according to Das et al. [11], $F = 0.6$ is in general a plausible initial choice, therefore such a value can be adopted in the *DE/current-to-best/1/bin*. Finally, eq. (10) is applied, which ensures that the components of the vector $\mathbf{V}_i^{it}$ are within the search space.

$$V_{i,j}^{it} = \begin{cases} V_{i,j}^{it}, & X_j^L \le V_{i,j}^{it} \le X_j^U \\ X_j^L, & V_{i,j}^{it} < X_j^L \\ X_j^U, & X_j^U < V_{i,j}^{it} \end{cases} \qquad j=1,\ldots,D \tag{10}$$

The crossover operation is necessary to increase the diversity of the population. It is done by combining the components of the vectors $\mathbf{X}_i^{it}$ and $\mathbf{V}_i^{it}$, which results in a new vector $\mathbf{U}_i^{it}$ [10]. To ensure that at least one component of $\mathbf{V}_i^{it}$ appears in $\mathbf{U}_i^{it}$, a random integer number mbr_i belonging to the interval $[1, D]$ is selected for each individual and, for this index, it leads to $U_{i,mbr_i}^{it} = V_{i,mbr_i}^{it}$. This whole process is described by eq. (11), where CR is the crossover rate.

$$U_{i,j}^{it} = \begin{cases} V_{i,j}^{it}, & if\ \mathcal{U}(0,1) \le CR\ or\ j = mbr_i \\ X_{i,j}^{it}, & otherwise \end{cases} \qquad j=1,\ldots,D \tag{11}$$

where $\mathcal{U}(0,1)$ represents a continuous uniform distribution, where a random variable takes values within the interval [0,1]. Here, the CR parameter of 0.9 is chosen for all variants in order to increase the diversity of the population.

Finally, in the selection stage, the value of the objective function (eq. (7)) is evaluated with the vectors $\mathbf{U}_i^{it}$ and $\mathbf{X}_i^{it}$. The vector that yields the smaller objective function value will compose the i_{th} position in the next population at iteration $it+1$, i.e.:

$$\mathbf{X}_i^{it+1} = \begin{cases} \mathbf{U}_i^{it}, & if\ S\left(\mathbf{U}_i^{it}\right) < S\left(\mathbf{X}_i^{it}\right) \\ \mathbf{X}_i^{it}, & otherwise \end{cases} \tag{12}$$

The numerous direct problems encountered throughout the evolution of the DE algorithm due to the change of the parameter vector $\mathbf{X}_i^{it}$ are numerically solved using the Finite Element Method (FEM) [12]. In this approach, the discrete weak form associated with eqs. (1)-(4) is expressed as follows:

$$\int_0^b \int_0^a w^h C\left(T^h\right) \frac{\partial T^h}{\partial t} dxdy + \int_0^b \int_0^a \left[\frac{\partial w^h}{\partial x} k_x\left(T^h\right) \frac{\partial T^h}{\partial x} + \frac{\partial w^h}{\partial y} k_y\left(T^h\right) \frac{\partial T^h}{\partial y} \right] dxdy = \int_0^a w^h \bar{q} dx + \int_0^b w^h \bar{q} dy \tag{13}$$

where the assumed solution for the temperature is given by $T(x,y,t) \approx T^h(x,y,t) = \sum_{j=1}^{n} N_j(x,y) T_j(t)$, whereas for the test function one assumes $w^h(x,y) = \sum_{i=1}^{n} N_i(x,y) w_i$ (Galerkin approach). Here, $N_j(x,y)$ are global interpolation functions, $T_j(t)$ are the unknown solutions at the nodes that are functions of time, and n stands for the total number of nodes in the mesh.

Substituting these approximations into the weak form (eq. (13)) and applying the initial condition (eq. (5)) across all nodes, the following system of nonlinear ODEs in the time domain arises:

$$\begin{cases} \mathbf{C}\left(\mathbf{T}(t)\right) \dfrac{d\mathbf{T}(t)}{dt} + \mathbf{K}\left(\mathbf{T}(t)\right) \mathbf{T}(t) = \mathbf{F}(t) \\ \mathbf{T}(0) = \mathbf{T}^0 \end{cases} \tag{14}$$

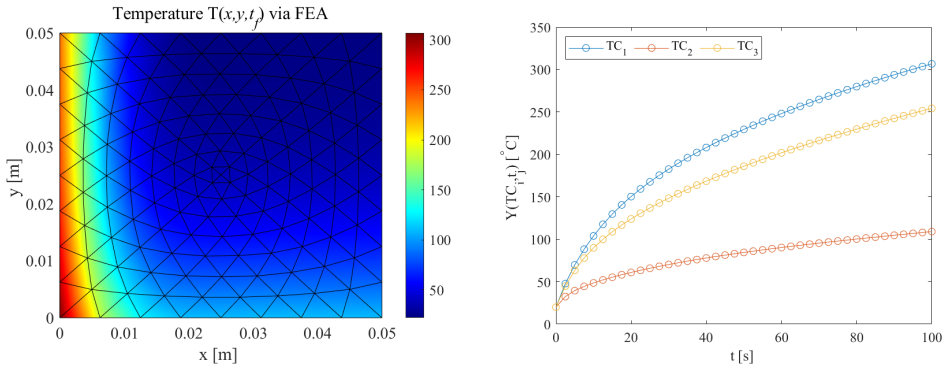
where $\mathbf{C}(\mathbf{T})$ and $\mathbf{K}(\mathbf{T})$ are, respectively, the capacitance and conductance matrices, which are dependent on the solution, while $\mathbf{F}(t)$ is the heat load vector that accounts for prescribed fluxes on the boundaries. Here, the implicit Euler method is combined with the Picard method to solve eq. (14) effectively. Therefore, the time domain is discretized into equal time intervals $[t_k, t_{k+1}]$ where $t_k = k\Delta t\,(k = 0, 1, 2, \ldots)$, whereas the nonlinearity is handled through the iterations $r = 0, 1, 2, \ldots$ for each time step. Thus, one obtains the following recurrence expression:

$$\underbrace{\left[\mathbf{C}\left(\mathbf{T}^{k+1,r}\right) + \Delta t \mathbf{K}\left(\mathbf{T}^{k+1,r}\right)\right]}_{\mathbf{K}_{eff}(\mathbf{T}^{k+1,r})} \mathbf{T}^{k+1,r+1} = \underbrace{\mathbf{C}\left(\mathbf{T}^k\right) \mathbf{T}^k + \Delta t \mathbf{F}^{k+1}}_{\mathbf{F}_{eff}(\mathbf{T}^k, \mathbf{F}^{k+1})}, \quad k = 0, 1, 2, \ldots; \; r = 0, 1, 2, \ldots \tag{15}$$

For each time step, the initial guess of the solution at the current time instant t_{k+1} is assumed to be the converged solution from the preceding time instant t_k, i.e., $\mathbf{T}^{k+1,0} = \mathbf{T}^k$. Afterwards, the iteration procedure for each time step is finished upon the convergence criterion $\frac{\left\|\mathbf{T}^{k+1,r+1} - \mathbf{T}^{k+1,r}\right\|}{\left\|\mathbf{T}^{k+1,r+1}\right\|} < \varepsilon$ is satisfied. The necessary steps integrating the FEA into the DE algorithm for conducting the inverse analysis are detailed in Alg. 1.

Algorithm 1 Algorithm for the inverse analysis

1: Set the dimension D of the problem, and the lower and upper bounds of each variable, i.e., $[X_j^L, X_j^U],\ j = 1, \ldots, D$.
2: Set the control parameters F_1, F_2, F_3, F_4 according to Table (1).
3: Set the crossover probability CR, and the maximal number of iterations it_{max}.
4: Randomly initialize the population $\mathbf{X}_i^1, i = 1, \ldots, N_{pop}$.
5: **for** it=1 to it_{max} **do**
6: **for** i=1 to N_{pop} **do**
7: *Mutation*: Apply eq. (9) with the corresponding F_k parameters of each DE variant. Additionally, ensure that $\mathbf{V}_i^{it}$ remains within the boundaries of the search space as defined by eq. (10).
8: *Crossover*: Generate the descendant individual $\mathbf{U}_i^{it}$ resultant from the crossing of $\mathbf{V}_i^{it}$ and $\mathbf{X}_i^{it}$ according to eq. (11).
9: *Selection*: Compute temperatures at the thermocouples for $\mathbf{X}_i^{it}$ and $\mathbf{U}_i^{it}$ by the nonlinear FEA (eq. (15)) and then evaluate the objective function values according to eq. (7) . Afterwards, apply eq. (12) to select the best individual to be added into the new population $\mathbf{X}_i^{it+1}$.
10: **end for**
11: **end for**



(a) (b)

Figure 2. Solution by the nonlinear FEA: a) temperature field at $t_f = 100s$; b) simulated measurements of temperature at the thermocouples.

4 Numerical results and discussion

The results were obtained according to the geometric parameters $a = b = 0.05m$ and the boundary and initial conditions of $\bar{q} = 25000Wm^{-2}$ and $T_0 = 20°C$, respectively [8]. In addition, the thermophysical properties of the orthotropic medium to be estimated (i.e., target values) are given in SI units as follows [3, 8]:

$$\mathbf{X}^* = \left[0.6081, 1.25 \times 10^{-3}, 4.752, 7.32 \times 10^{-3}, 1.7 \times 10^{6}, 2.608 \times 10^{3}\right] \tag{16}$$

where k_{x1} is one order of magnitude greater than that adopted in Sawaf et al. [8], and it is comparable to that used in Kim et al. [3].

An in-house MATLAB code was developed to carry out the nonlinear transient finite element analysis, and, for this example, a time-step size of $\Delta t = 2.5s$, a total of $N_t = 40$ time steps, and a tolerance of $\varepsilon = 10^{-8}$ were adopted. Taking into account $\mathbf{X}^*$, this code was also used to generate the simulated measurements employed in the inverse analysis. In this way, the nonlinear finite element code is coupled with the DE one to compute the objective function, and twenty distinct runs were performed for each of the three differential evolution variants described in the text (it is worth mentioning that tuning of the DE parameters is beyond the scope of this work). The maximum number of iterations and the population size per run were set to $it_{max} = 800$ and $N_{pop} = 60$, respectively. The search space is defined such that the constraints are readily satisfied according to the following bound vectors:

$$\mathbf{X}^L = \left[0.1, 0, 0.1, 0, 10^5, 0\right]; \quad \mathbf{X}^U = \left[10, 0.1, 10, 0.1, 10^7, 10^4\right] \tag{17}$$

Fig. 2 shows the temperature field at the end time of the analysis adopting a mesh with 256 linear triangle elements, along with the temperature records at the thermocouple locations, where the influence of the orthotropic medium is clearly evident in the temperature profiles. Initially, experiments were performed without adding noise to the simulated experimental data. Then, measurement errors are simulated by adding a Gaussian error term to the noiseless data as:

$$Y\left(TC_i, t_j\right) = Y_{noiseless}\left(TC_i, t_j\right) + \omega_{ij}\sigma, \; i = 1, \ldots, N_s; \; j = 1, \ldots, N_t \tag{18}$$

where ω_{ij} is a random number that follows a Gaussian distribution over the interval [-2.576, 2.576] corresponding to a 99% confidence level for the measured data. The standard deviation of the temperature measurement error by the thermocouples is considered constant and equal to $\sigma = 0.3^0C$ obtained experimentally according to Kim et al. [3].

One can observe the faster convergence of the *DE/current-to-best/1/bin* in Fig. 3, which displays the mean value of the objective function across all runs, in relation to the other variants. It is also possible to verify the slower convergence of the *DE/rand/1/bin* and the inferior performance of the *DE/best/1/bin* even with noise-free data. Furthermore, according to Table 2[1], the *DE/current-to-best/1/bin* stands out once again with the lowest values of the objective function, and the lowest standard deviation in the order of 10^{-17} for the data without noise and 10^{-13} for the data with noise.

[1]Bold face numbers indicate the best results.

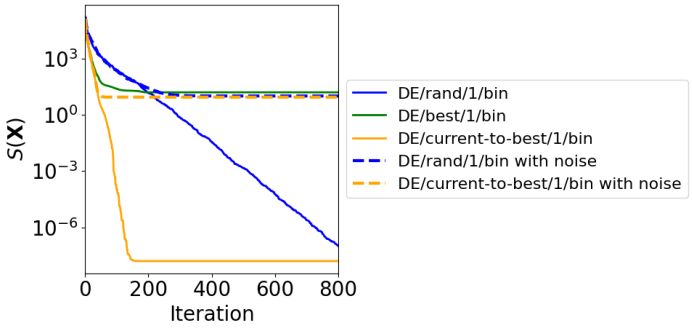


Figure 3. Comparison of mean values of the objective function during the iterations.

This last fact is an indication of the effectiveness of this variant, unlike the *DE/best/1/bin* that presents a low value for the objective function, but a high standard deviation, as well as the *DE/rand/1/bin*, which obtained a slightly higher objective function value, but a standard deviation in the order of 10^{-7}.

Table 2. Comparison of the statistical results.

	Best	Mean	Worst	Std.
DE/rand/1/bin	1.9936×10^{-8}	1.0251×10^{-7}	2.9711×10^{-7}	7.6172×10^{-8}
DE/best/1/bin	1.5931×10^{-8}	1.5827×10^{1}	7.1927×10^{1}	2.9483×10^{1}
DE/current-to-best/1/bin	$\mathbf{1.5931 \times 10^{-8}}$	$\mathbf{1.5931 \times 10^{-8}}$	$\mathbf{1.5931 \times 10^{-8}}$	$\mathbf{4.2802 \times 10^{-18}}$
DE/rand/1/bin with noise	8.7838	1.0079×10^{1}	3.4699×10^{1}	5.7948
DE/current-to-best/1/bin with noise	**8.7838**	**8.7838**	**8.7838**	$\mathbf{8.1532 \times 10^{-14}}$

Finally, Table 3[2] shows similarities in relation to relative errors in estimating the $\mathbf{X}$ components of the *DE/rand/1/bin* and *DE/current-to-best/1/bin* variants with noise-free data. However, when using these variants with noisy simulated data, the *DE/current-to-best/1/bin* performed better than the *DE/rand/1/bin* in estimating all components. Therefore, there are indicators of the superiority of the *DE/current-to-best/1/bin* variant compared to *DE/rand/1/bin* and *DE/best/1/bin* ones for the problem studied.

Table 3. Comparison of the estimated mean values for the parameters.

	rand/1	*best/1*	*current/1*	*rand/1 (noise)*	*current/1 (noise)*
k_{x0}	$\mathbf{6.0810 \times 10^{-1}}$	6.4111×10^{-1}	$\mathbf{6.0810 \times 10^{-1}}$	6.1450×10^{-1}	$\mathbf{6.1134 \times 10^{-1}}$
Error$_{k_{x0}}$ (%)	**0.000**	5.428	**0.000**	1.052	**0.533**
k_{x1}	$\mathbf{1.249 \times 10^{-3}}$	9.648×10^{-4}	$\mathbf{1.249 \times 10^{-3}}$	1.158×10^{-3}	$\mathbf{1.190 \times 10^{-3}}$
Error$_{k_{x1}}$ (%)	**0.080**	22.816	**0.080**	7.360	**4.800**
k_{y0}	$\mathbf{4.7520 \times 10^{0}}$	4.9883×10^{0}	$\mathbf{4.7520 \times 10^{0}}$	4.8150×10^{0}	$\mathbf{4.7769 \times 10^{0}}$
Error$_{k_{y0}}$ (%)	**0.000**	4.973	**0.000**	1.326	**0.524**
k_{y1}	$\mathbf{7.319 \times 10^{-3}}$	5.489×10^{-3}	$\mathbf{7.319 \times 10^{-3}}$	6.564×10^{-3}	$\mathbf{6.910 \times 10^{-3}}$
Error$_{k_{y1}}$ (%)	**0.014**	25.014	**0.014**	10.328	**5.601**
C_0	$\mathbf{1.69 \times 10^{6}}$	1.61×10^{6}	$\mathbf{1.69 \times 10^{6}}$	1.67×10^{6}	$\mathbf{1.68 \times 10^{6}}$
Error$_{C_0}$ (%)	**0.588**	5.294	**0.588**	1.765	**1.176**
C_1	$\mathbf{2.6080 \times 10^{3}}$	3.5964×10^{3}	$\mathbf{2.6080 \times 10^{3}}$	2.9663×10^{3}	$\mathbf{2.8175 \times 10^{3}}$
Error$_{C_1}$ (%)	**0.000**	37.899	**0.000**	13.738	**8.033**

[2]Bold face numbers indicate the best results.

5 Conclusions

The primary motivation of this study was to assess the performance of three widely used variants of the Differential Evolution (DE) algorithm, namely, *DE/rand/1/bin*, *DE/best/1/bin* and *DE/current-to-best/1/bin* in an inverse analysis to estimate the thermal conductivities and heat capacity of an orthotropic medium. The transient nonlinear heat conduction model in a plate was straightforwardly solved by the Finite Element Method (FEM) considering the implicit Euler scheme and Picard iteration procedure. Numerical experiments indicated that the *DE/current-to-best/1/bin* variant outperformed the other two, both in statistical metrics and computational efficiency, requiring fewer iterations and, consequently, reducing the number of objective function evaluations, which are highly costly.

Acknowledgements. The authors acknowledge support of CAPES, CNPq and UFSJ/PPMEC/DCTEF.

Authorship statement. The authors hereby confirm that they are the sole liable persons responsible for the authorship of this work, and that all material that has been herein included as part of the present paper is either the property (and authorship) of the authors, or has the permission of the owners to be included here.

References

[1] M. M. Mejias, H. R. B. Orlande, and M. N. Ozisik. A comparison of different parameter estimation techniques for the identification of thermal conductivity components of orthotropic solids. *IEEE Transactions on Evolutionary Computation*, 2014.
[2] L. Yang, B. Sun, and X. Sun. Inversion of thermal conductivity in two-dimensional unsteady-state heat transfer system based on finite difference method and artificial bee colony. *Applied Sciences*, vol. 9, n. 22, 2019.
[3] S. K. Kim, B. S. Jung, H. J. Kim, and W. I. Lee. Inverse estimation of thermophysical properties for anisotropic composite. *Experimental Thermal and Fluid Science*, vol. 27, n. 6, pp. 697–704, 2003.
[4] M. J. Colaço, H. R. Orlande, and G. S. Dulikravich. Inverse and optimization problems in heat transfer. *Journal of the Brazilian Society of Mechanical Sciences and Engineering*, vol. 28, pp. 1–24, 2006.
[5] S. Somasundharam and K. Reddy. Inverse analysis for simultaneous estimation of temperature dependent thermal properties of isotropic materials. *Thermal Science and Engineering Progress*, vol. 20, pp. 100728, 2020.
[6] X. Wang, H. Li, L. He, and Z. Li. Evaluation of multi-objective inverse heat conduction problem based on particle swarm optimization algorithm, normal distribution and finite element method. *International Journal of Heat and Mass Transfer*, vol. 127, pp. 1114–1127, 2018.
[7] J. P. Rocha, F. S. Loureiro, H. S. Bernardino, A. B. Vieira, and H. J. Barbosa. Metaheuristics applied to the thermographic detection of multicentric breast tumor. *Journal of the Brazilian Society of Mechanical Sciences and Engineering*, vol. 46, n. 6, pp. 361, 2024.
[8] B. Sawaf, M. Ozisik, and Y. Jarny. An inverse analysis to estimate linearly temperature dependent thermal conductivity components and heat capacity of an orthotropic medium. *International Journal of Heat and Mass Transfer*, vol. 38, n. 16, pp. 3005–3010, 1995.
[9] K. V. Price, R. M. Storn, and J. A. Lampinen. *Differential evolution: a practical approach to global optimization*. Springer, 2005.
[10] J. Qiang and C. E. Mitchell. A unified differential evolution algorithm for global optimization. *IEEE Transactions on Evolutionary Computation*, 2014.
[11] S. Das, A. Abraham, and A. Konar. *Differential Evolution Algorithm: Foundations and Perspectives*, pp. 63–110. Springer Berlin Heidelberg, Berlin, Heidelberg, 2009.
[12] R. W. Lewis, K. Morgan, H. Thomas, and K. N. Seetharamu. *The finite element method in heat transfer analysis*. John Wiley & Sons, 1996.